Anal. Chem. **1999,** *71,* 5413–5419

Evaluation of Metal Migration and Determination of Trace Metals after Microwave Digestion for Lithographic Materials

Fu-Hsiang Ko,*,† Mei-Ya Wang,‡ and Tien-Ko Wang‡

National Nano Device Laboratories, National Chiao Tung University, Hsinchu 300, Taiwan, and Department of Engineering and System Science, National Tsing Hua University, Hsinchu 300, Taiwan

The radioactive tracer technique was applied to investigate the migration of cesium and zinc impurities from bottom antireflective coating (BARC) and photoresist (PR) into underlying substrate. The effects of normal baking temperatures and substrate types were studied. Our results indicated that BARC has higher migration ratios than PR, irrespective of the substrate types and normal baking temperatures. The substrate type did not appear to strongly affect the metal migration ratios. However, water and/or solvent evaporation due to temperature change was found to have a significant effect on metal migration. The diffusion profiles of BARC and PR were depicted based on diffusion equations and the migration ratios. Both the UV/visible spectrometric and the gravimetric methods were successfully implemented to evaluate the feasibility of closed-vessel microwave digestion efficiency for BARC and PR samples. By following the established microwave digestion method and the inductively coupled plasma mass spectrometer (ICPMS) determination, the detection limits obtained for multielements were in the ppb and sub-ppb levels. Except for calcium, the spike recoveries of metals ranged from 91 to 132% and 87 to 125% for BARC and PR, respectively. The analytical results were found to be in reasonably good agreement with the literature values.

The increasing complexity and miniaturization of modern integrated circuits demand a higher device yield, hence decreasing the defect density in the active region of silicon devices.[1] For a deep submicrometer device, metal precipitates could cause a distortion of the resultant electrical properties and may result in faulty integrated circuits.[2–5] For example, metals can degrade the dielectric properties of gate oxide, leading to premature breakdown. They can also diffuse into the bulk of the silicon substrate, resulting in increased junction leakage as well as reduced minority carrier lifetime. Therefore, a more thorough understanding of the potential of metal diffusions into the silicon substrate during device fabrication is essential to reduce contamination and to enhance circuit yield.

The control of fabrication processes involved in device manufacturing has become crucial due to the growing complexity of materials and tools. Among these processes, lithography plays a very important role because it is applied repeatedly to the wafer surface during device manufacturing. Knowledge of the behavior of metallic contaminants in lithographic materials and their migration into the underlying substrate is imperative to gain proper control of impurity concentration in the "high-purity" lithographic materials, which is an important issue for fast proliferation of lithography process in the IC industry in the coming years.[6] Although it is always safer to demand an unnecessarily high degree of purity for lithographic materials, the cost could be exceedingly expensive and unnecessary.

Evaluation of the ratios of metallic impurities migrating from deep ultraviolet (DUV) bottom antireflective coating (BARC) or photoresist (PR) into the underlying substrate during lithographic processing (e.g., baking) requires various analytical methods[7–11] for determining the impurity concentration in the resist layer and in the underlying substrate. Among these analytical methods, the radioactive tracer technique[12–14] has been proven to be very suitable for studying element migration in materials, environment, and biochemistry. The advantages of the radioactive tracer technique include high throughput, ease of operation, interference-free from the stable isotope, and a high degree of reliability. Despite the versatility of the radioactive tracer technique, however,

* Corresponding author: (telephone) +886-35726100, ext 7618; (fax) +886-35713403; (e-mail) fhko@ndl.gov.tw.

(1) Sze, S. M. *VLSI Technology*; McGraw-Hill: New York, 1988; Chapter 14.
(2) Chang, C. Y.; Sze, S. M. *ULSI Technology*; McGraw-Hill: New York, 1996; Chapter 12.
(3) Ward, P. J. *J. Electrochem. Soc.* **1982**, *129*, 2573–2575.
(4) Miyazaki, M.; Sano, M.; Sumita, S.; Fujino, N. *Jpn. J. Appl. Phys.* **1991**, *30*, L295–L297.
(5) Rotondaro, A. L. P.; Hurd, T. Q.; Kaniava, A.; Vanhellemont, J.; Simoen, E.; Heyns, M. M.; Claeys, C. *J. Electrochem. Soc.* **1996**, *143*, 3014–3019.
(6) *The National Technology Roadmap for Semiconductors*; Semiconductor Industry Assoc., San Jose, CA, 1997; p 93.
(7) Crighton, J. S.; Carroll, J.; Fairman, B.; Haines, J.; Hinds, M. *J. Anal. At. Spectrom.* **1997**, *12*, 509R–542R.
(8) Fuchs-Pohl, G. R.; Solinska, K.; Feig, H. *Fresenius J. Anal. Chem.* **1992**, *343*, 711–714.
(9) Argentine, M. D.; Barnes, R. M. *J. Anal. At. Spectrom.* **1994**, *9*, 1371–1378.
(10) Shabani, M. B.; Yoshihiro, T.; Abe, H. *J. Electrochem. Soc.* **1996**, *143*, 2025–2029.
(11) Dowsett, M. G.; Barlow, R. D.; Allen, P. N. *J. Vac. Sci. Technol.* **1994**, *B12*, 186–198.
(12) Borg, R. J.; Dienes, G. J. *An Introduction to Solid State Diffusion*; Academic Press: Boston, 1988; Chapter 11.
(13) Glekas, I. P. *Water Sci. Technol.* **1995**, *32*, 179–187.
(14) Choppin, G. R.; Rydberg, J. *Nuclear Chemistry*; Pergamon Press: Oxford, U.K., 1980; Chapter 18.

10.1021/ac9906779 CCC: $18.00 © 1999 American Chemical Society
Published on Web 10/29/1999

it has not been applied to study metal migrations between the lithographic materials and the underlying substrates.

Currently, determination of ultratrace elements of lithographic materials by vendors or advanced semiconductor device manufacturers generally uses the graphite furnace atomic absorption spectrometry (GFAAS). In this method, the sample is digested with the acid mixture in a beaker on a hot plate.[15] However, throughput and contamination are important issues to be questioned with the methods. Plasma-based instruments, such as inductively coupled plasma mass spectrometry (ICPMS) and inductively coupled plasma optical emission spectrometry (ICP-OES), possess the advantage of simultaneous multielement capability. However, they require a rapid, efficient, and reliable sample preparation technology to ensure their efficiency and capability. This is because the plasma-based instruments easily suffer from matrix-induced spectral overlap problems and matrix-induced signal intensity changes as a consequence of incomplete sample dissolution.[16]

It has been reported[17] that closed-vessel microwave decomposition of biological samples with acid at elevated temperatures and pressures could rapidly destroy the organic matrix. Under these conditions, the oxidizing power of the acid is significantly increased, and the degree of contamination, loss of volatile elements, and dissolution time are significantly reduced.

In this work, the radioactive tracer technique was proposed to investigate the migration ratios of Cs and Zn impurities from DUV BARC and PR into the underlying substrate. The effects of baking temperatures and the types of underlying surfaces were also discussed. In addition, possible mechanisms involved in metal migration were discussed. Furthermore, both UV/visible absorption and total dry residual method were studied for evaluating the digestion efficiency of the lithographic materials. A suitable digestion recipe was found and was subsequently employed to destroy the complex matrix for lithographic materials. Then, the digestion solution after acid evaporation was analysis with ICPMS.

EXPERIMENTAL SECTION

Materials. P-type ⟨100⟩ wafers of 15-cm diameter were passivated with various films (i.e., polysilicon, silicon dioxide, silicon nitride). Nonpassivated or bare silicon was used as a control. The wafers were cut into pieces, 2 cm by 2 cm in area, to serve as test samples. These test samples were prepared through various lithographic processes to study the behavior of contaminants introduced during the lithographic processes. Carrier-free radioactive tracers from DAMRI were used in this study. The tracer composition was 10 μg/g $^{137}CsCl$ (0.747 M Bq/g) and 10 μg/g $^{65}ZnCl_2$ (0.857 M Bq/g) in 0.1 M hydrogen chloride solution.

The lithographic materials used in this work were DUV BARC of AZ KrF-12 (Clariant) and DUV PR of SEPR-401H (Shin-Etsu Chemical). The photoresist stripper was 1-methyl-2-pyrrolidone (NMP) obtained from E. Merck (Darmstadt, Germany).

All reagents used were of analytical or higher grade from E. Merck. High-purity water, which was sequentially purified by demineralization, two-stage quartz distillation, and sub-boiling distillation, was used throughout this study. Nitric acid (E. Merck; Tracepure grade, further treated by in-house sub-boiling), sulfuric acid (Fisher Scientific, Pittsburgh, PA; Trace metal grade), hydrogen peroxide (E. Merck), and hydrochloric acid (E. Merck) were used for digestion of the samples. Standard solutions of the analytes in 1% nitric acid were freshly prepared by diluting the concentrated (1000 mg/L) stock solutions (E. Merck).

Film Growing Process. To prepare different underlying surfaces for this study, films of polysilicon, silicon oxide, and silicon nitride were deposited onto various starting silicon wafers by a low-pressure, chemical-vapor-deposited (LPCVD) method in a quartz reactor. The polysilicon film was deposited with silane gas (SiH_4) at 60 sccm and 620 °C. The silicon oxide layer was grown by wet oxidation with a gas mixture of hydrogen (8 slm) and oxygen (4999 sccm) at 978 °C. The silicon nitride film was deposited with a gas mixture of ammonium (130 sccm) and dichlorosilane (SiH_2Cl_2, 30 sccm) at 780 °C.

Afterward, wafers were cut into 2 cm × 2 cm pieces to serve as test samples, and a BARC or PR layer was then coated onto these test samples. This procedure was accomplished by holding the test wafer by a vacuum chuck, and then 1 mL of radioactive DUV BARC or PR was dispensed onto the sample surface by a pipet. The coating processes of DUV BARC and PR were performed by spinning the samples at 1500 rpm for 0.5 min. The BARC samples were then baked at 180 °C for 1 min on a hot plate, while the PR samples were baked at 80, 100, and 120 °C for 2 min.

Radioactive Tracer Experimental Procedure. To prepare the radioactive DUV PR and BARC, one volume of diluted radioactive tracer (in 0.005 M HCl) was mixed with five volumes of lithographic materials. The radioactive lithographic solution was well-shaken to ensure a homogeneous state and was applied to the test samples by the spin-coating process mentioned above. After solvent evaporation, the test sample was counted with a high-resolution γ-ray spectrometer. The counting system features an HPGe detector coupled with multichannel analyzer (Canberra AccuSpec) and the usual electronics. The energy resolution of the system was 2.4 keV at 1332 keV. The intensity of γ-ray for ^{137}Cs ($t_{1/2} = 30.15$ y) and ^{65}Zn ($t_{1/2} = 243.9$ d) was monitored at the energy levels of 661.7 and 834.8 keV, respectively. After counting, the BARC or PR layer was removed by immersing in a 100-mL NMP solution at 60 °C for 5 min, followed by drying on a hot plate. The radioactivity of metal on the wafer was checked by the same HPGe detection system. The counting time was adjusted and elongated to minimize counting errors for lower radioactivity. The migration ratios of Cs and Zn from lithographic materials into the underlying substrate were determined by the ratio of the time-average counts after and before film stripping.

Microwave Digestion and Sample Analysis. Microwave digestion of lithographic materials was accomplished by placing the closed vessels inside a commercial oven. The closed vessel (model MDS-2000, CEM, Matthews, NC) was equipped with a Teflon-coated cavity and a removable 12-position sample carousel. The oven had a variable power range (up to 630 W) adjustable in 1% increments. The existing turntable was rotated at 3.5 revolutions/min, and a pressure line was installed with a transducer for monitoring pressure. The pressure limit was set at 150 psi. As the pressure in the vessel exceeded the pressure limit, the oven

(15) Takenaka, M.; Kozuka, S.; Hashimoto, Y. *Bunseki Kagaku* **1993**, *42*, T71–T75.
(16) Kingston, H. M. *At. Spectrosc.* **1998**, *19*, 27–30.
(17) Ko, F.-H.; Yang, M.-H. *J. Anal. At. Spectrom.* **1996**, *11*, 413–420.

power was automatically turned off. When the pressure dropped below 148 psi, the oven would restart to heat the sample. The sample was digested in a lined digestion vessel (volume, 100 mL; maximum operating pressure, 200 psi) consisting of a chemically resistant inner liner (Teflon PFA) and a cover to contain and isolate the sample solution from a higher strength outer pressure vessel body (Ultem polyetherimide). To protect the digestion vessel from excessive pressures, a rupture membrane (Part No. 324350, CEM) was used to direct the escape gases through the exhaust port if the safety rupture membrane broke.

A 0.25-mL aliquot of lithographic material was digested in the closed-vessel microwave oven. Recipes of various digestion programs were attempted to determine the best dissolution condition. Upon completion of microwave digestion, the sample was cooled before transferring to another Teflon beaker. The sample solution was heated with a quartz hot plate on a clean bench (class 100) to evaporate until incipient dryness, and subsequently 5 mL of 1% nitric acid was added. The solution can be used for evaluation of the completeness of the digestion process by UV/visible spectrometry or for the determination of the metals using the ICPMS (Perkin-Elmer Sciex Elan 5000, Norwalk, CT) and ICP-OES (Perkin-Elmer, Optima 3000). An alternative method for evaluating the digestion efficiency was to weigh the total dry residual solid after and before sample digestion and complete reagent evaporation.

RESULTS AND DISCUSSION

Metal Migrations for DUV BARC and PR. In general, a basic lithographic process includes resist-coating, soft bake, exposure, postexposure bake, development, and hard bake.[18] One of the lithographic materials, namely, DUV PR, can be used to define the pattern of critical layer. However, Bencher and co-workers[19] reported numerous problems associated with optical proximity effect, this phenomenon only observed for the PR layer during the exposure process. These problems include interference, reflective notching, and standing waves. Therefore, to minimize these problems, it becomes necessary to apply a BARC layer to be coated between the PR and the underlying layer.[20] The baking procedure, usually applied after coating BARC or PR, can stabilize and solidify the coating layers. Since the metals in BARC or PR could migrate into the substrate during the baking process, it is important to determine the amounts of migrating metals to ensure process reliability.

Since limited analytical methods are available for determining metal migrations, we propose the radioactive tracer technique mentioned in Experimental Section to explore the migration ratios. Table 1 summarizes the migration ratios of Cs and Zn impurities from DUV BARC and PR into various underlying substrates at normal baking temperatures (i.e., 180 °C for BARC and 100 °C for PR). It should be noted that the migration ratios in BARC were significantly higher than in PR, regardless of the substrate types. There are three reasons that can be used to explain the different trends of migration ratios. The first is related to the temperature

Table 1. Migration Ratios for Impurities Transported from BARC and PR into Underlying Substrates at Various Baking Temperatures

substrate	element	BARC 180 °C, %	PR 80 °C, %	PR 100 °C, %	PR 120 °C, %
bare silicon	Cs	20.0	1.9	2.3	2.9
	Zn	18.3	4.9[a]	2.7[a]	1.6[a]
polysilicon	Cs	46.2	0.9	2.5	3.1
	Zn	25.8	2.3[a]	1.3[a]	0[a]
silicon oxide	Cs	13.4	0.7	0.8	1.4
	Zn	35.5	5.6[a]	4.6[a]	0[a]
silicon nitride	Cs	17.3	3.9	3.2	2.6
	Zn	26.2	0[a]	0[a]	0[a]

[a] The data were obtained from ref 21.

effect on metal diffusion. The diffusion coefficient (D) and diffusion length (L) for various metals can be simplified and described by the equations as follows:[21]

$$D = D_0 e^{-E_a/kT} \quad (1)$$

$$L = \sqrt{Dt} \quad (2)$$

where D_0 is the preexponential factor dependent on the vibration frequency of atoms in the layers, T is the diffusion temperature (in kelvin), E_a is related to the height of the energy barrier at such sites, k is the Boltzmann constant, and t is the diffusion time. It should be noted that the baking temperature of BARC at 180 °C was significantly higher than PR at 100 °C. Therefore, the higher diffusion coefficient and diffusion length, described in eqs 1 and 2, led to the higher diffusion ratios for metals in the BARC layer as compared with metals in the PR layer.

The second explanation is associated with the film structure. The films of BARC and PR can be treated as the amorphous polymer layer after the normal baking procedure. Taking the layer density or porosity into consideration, the observation explains the fact that the BARC layer structure is more porous and less dense as compared with PR layer. Therefore, the metals migrate across the BARC layer with less hindrance. The third is related to the thickness of the coating layer. The thickness of BARC layer is only one-tenth of the PR layer. Therefore, the metal migration ratios are significantly higher than in PR layer. Also, this result is correlated with the diffusion profile depicted in next section.

It was also observed from Table 1 that the migration ratios in BARC ranged from a lowest value (13.4% for Cs in silicon oxide) to a highest value (46.2% for Cs in polysilicon). The values are substantially higher in comparison with those in the PR layer (all below 6%), indicating that contamination of metals from the BARC layer cannot be neglected for any substrate types. Therefore, it can be concluded that maintaining high degree of purity for the incoming BARC material is critical to ensure the reliable process fabrication for device manufacturer. Interestingly, it was found that the migration ratios for PR did not exhibit strong temperature dependence as the baking temperature was elevated from 80 to

(18) Thompson, L. F.; Willson, C. G.; Bowden, M. J. *Introduction to Microlithography*, 2nd ed.; American Chemical Society: Washington, DC, 1994; Chapter 4.
(19) Bencher, C.; Ngai, C.; Roman, B.; Lian, S.; Vuong, T. *Solid State Technol.* **1997**, (Mar) 109–114.
(20) Tanaka, T.; Hasegawa, N.; Shiraishi, H.; Okazaki, S. *J. Electrochem. Soc.* **1990**, *137*, 3900–3904.
(21) Wang, M.-Y.; Ko, F.-H.; Wang, T.-K.; Yang, C.-C.; Huang, T.-Y. *J. Electrochem. Soc.* **1999**, *146*, 3455–3460.

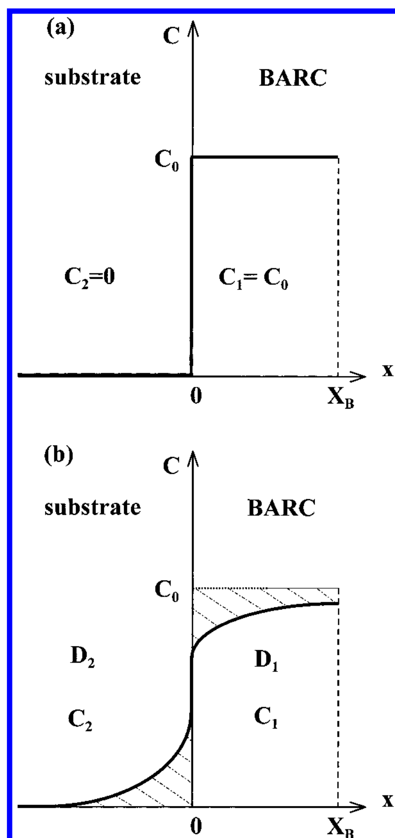

Figure 1. Metal diffusion profile (X_B, thickness of the layer) of BARC sample: (a) initially and (b) after baking.

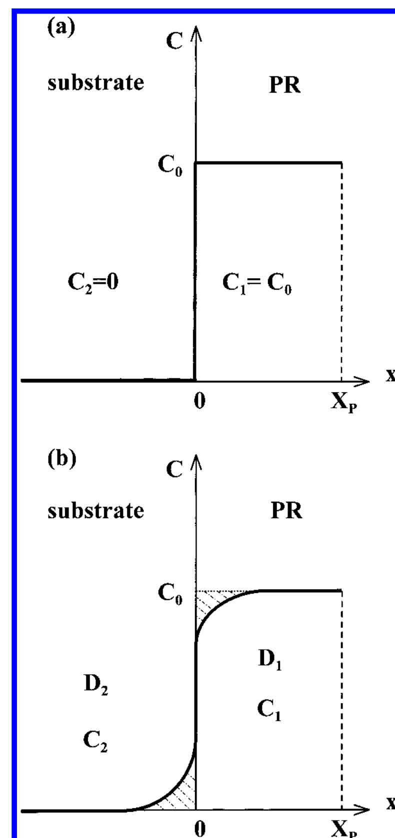

Figure 2. Metal diffusion profile (X_P, thickness of the layer) of PR sample: (a) initially and (b) after baking.

120 °C. In the PR layer, the migration ratios for Cs increased with temperature for the substrates of bare silicon, polysilicon, and silicon oxide, whereas the opposite tendency can be observed for silicon nitride. As for Zn, the migration ratios decreased with temperature regardless of the substrate types.

If we only consider eqs 1 and 2, the migration ratios should increase with increasing temperature. However, the experimental results based on the radioactive tracer method did not follow this hypothesis, implying that another factor may have affected the metal behavior. This factor can be attributed to the change of component in the PR layer. As the metallic ions are solvated with the residual water and/or photoresist solvent to form $M(H_2O)_x^{n+}$ and/or $M(solvent)_x^{n+}$, the baking temperature induces the water and/or solvent to evaporate at a distance far away from the substrate. Taking the effects of metal diffusion and water/solvent evaporation into consideration, the migration ratio of the metals changes with temperature can be classified into four types. Type I describes the condition when the effect of metal diffusion dominates while the effect of water/solvent evaporation is negligible; as a result, the migration ratio increases as temperature goes up. Type II is when water/solvent evaporation dominates while the effect of metal diffusion is insignificant; therefore, the migration ratio decreases as temperature goes up. Type III has a turnover temperature. If the baking temperature is lower than the turnover temperature, it behaves like type I; whereas, when the baking temperature is higher than the turnover temperature, it behaves like type II. Type IV shows the opposite tendency as compared with type III.

Based on the proposed four types of migration model, the experimental results appearing in Table 1 can be realized. The tendency of Cs migration for substrates of bare silicon, polysilicon, and silicon nitride belongs to type I, whereas for silicon nitride it belongs to type II. It is found the Zn has type II migration regardless of substrate types. The migration ratio for Zn in silicon nitride substrate is null, which is the special case of type II. This observation indicates the water/solvent evaporation can effectively restrict the Zn impurity from reaching the silicon nitride substrate.

For ease of spiking the commercial radioactive tracers into the lithographic materials, the metal migration ratio is obtained from the polymer solution containing radioactive tracers by combining aqueous and lithographic materials to give a mixture. By following the procedure given in the Experimental Section, the water/solvent content of the lithographic materials is higher than the unadulterated lithographic material. According to our proposed migration model, the migration ratio is underestimated due to the water/solvent effect. Therefore, the metal migration problem for original lithographic materials (e.g., PR and BARC) will induce contamination during baking process.

Metal Diffusion Profiles. To describe the metal diffusion profiles for BARC and PR, a semiempirical one-dimensional diffusion model, depicted in Figures 1 and 2, is employed. The initial concentration of metals in the coating layer is assumed to be C_0 at various cross sections. Equations 3 and 4, which describe the relationship for the metals in the layers and in the substrates at time t and location x, can be expressed as follows:[22]

(22) Crank, J. *The Mathematics of Diffusion*; Oxford Univ. Press: London, 1976; Chapter 3.

$$\partial C_1/\partial t = D_1(\partial^2 C_1/\partial x^2) \quad (3)$$

$$\partial C_2/\partial t = D_2(\partial^2 C_2/\partial x^2) \quad (4)$$

where C_1 and C_2 denote the concentrations of metals in the coating layer and in the underlying substrate, respectively. D_1 and D_2 are the diffusion coefficients for the metals in the corresponding layers.

Figure 1 illustrates the metal diffusion profiles between the BARC layer (X_B, thickness of 75 nm) and the substrate. Figure 1a shows the initial profile of metal, while Figure 1b represents the concentration profile after diffusion/baking. The higher migration ratios found in Table 1 imply that the cross-sectional concentration (C_1) over the whole thickness should decrease after normal baking. The shadow areas, representing the amount of diffusion metal, in either side of the interface are equal. A different trend is seen for the PR layer (X_P , thickness of 750 nm) as displayed in Figure 2. Figure 2a shows the initial profile of metal, while Figure 2b represents the concentration profile after diffusion/baking. Due to the limited migration ratio (<6%), the metal concentrations in locations away from the interface should remain constant (C_0). Also, the shadow areas on either side of the interface are equal for the PR sample. It should be noted that the diffusion ratio could be calculated from the ratio of the shadow area (right side for BARC in Figure 1b, or PR in Figure 2b) and the area below the initial profile (right side for BARC in Figure 1a, or PR in Figure 2a).

Evaluation of Digestion Efficiency. The previous sections have clearly described the extent of metal migrations and their diffusion profiles for lithographic materials. For the purpose of controlling contamination of BARC and PR, the concentration of metals in both materials should be determined. However, since the materials contain complex polymers and organic compounds, the direct determination methods may suffer from serious matrix interference effect. For example, the complex and viscous characteristics of such materials can severely clog the sample loop or the interface of the measuring instrument, thus affecting the analytical reliability. Therefore, it is inevitable to develop a suitable pretreatment method for metal determination. Destruction of the organic matrix with closed-vessel microwave digestion is usually used for trace and ultratrace analysis. However, the extent of the matrix destruction by a specific decomposition method has seldom been evaluated quantitatively. Conventionally, when clear and colorless solutions are obtained, or when total recovery of some elements is obtained, it is assumed that oxidation of the organic matters has been completed for all practical purposes. However, such assumptions are not necessarily reliable in all cases. More conclusive and direct information on the presence and identities of residual matter retained by the acid dissolution is certainly desirable, especially if such matter could interfere with the subsequent measurement.

In this study, both the UV/visible spectrometric and gravimetric methods were tested for their applicabilities to evaluate the completeness of the sample matrix destruction with various digestion recipes and programs. Lithographic materials containing various types of polymers and other organic compounds exhibit distinct absorption spectra in the UV/visible region. Destruction of the organic matrix may, consequently, result in a decrease in the intensity of UV/visible absorption. Therefore, measurement of the decreasing absorption of the digested sample can provide useful information to evaluate the effectiveness of sample decomposition. Figure 3 shows the UV/visible absorption spectra from 200 to 500 nm for the BARC and the PR samples before and after digestion by closed-vessel microwave digestion. The digestion programs and reagents are listed in Table 2. Figure 3a shows that the BARC sample (diluted 1:10000) exhibited strong absorption at 200−240 nm, while the sample after program 1 (only 1.5 mL of HNO_3) digestion still exhibited strong absorption between 200 and 220 nm. This indicated that the program 1 digestion method was not effective and that the residual pressure after digestion should be found at 85−100 psi. However, if the closed vessel is opened, and followed with step 2 by spiking with 0.5 mL of H_2O_2 (i.e., program 2), the absorption in the same wavelength region was appreciably lowered. This may provide a preliminary indication of the effectiveness of this digestion procedure for BARC.

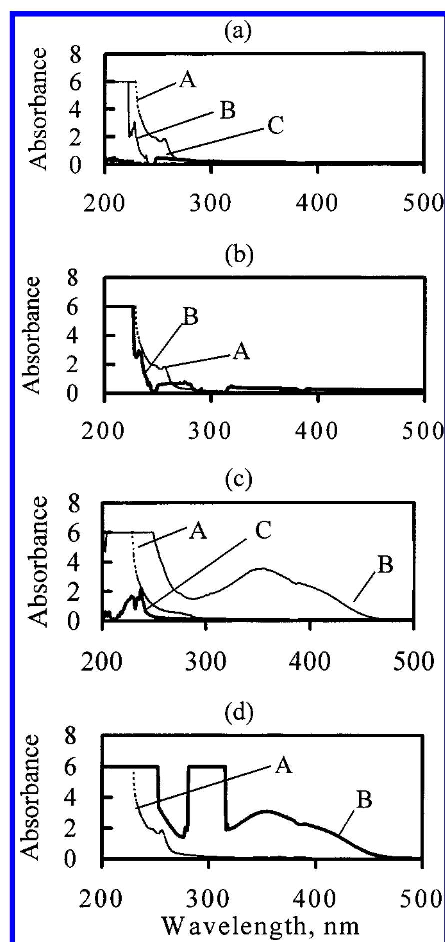

Figure 3. UV/visible absorbance spectra of closed-vessel microwave digestion: (a) BARC samples, where A is original BARC (1:10000 dilution), B is BARC sample after program 1 digestion (1:500 dilution), and C is BARC after program 2 digestion (1:60 dilution); (b) BARC samples, where A is original BARC (1:10000 dilution) and B is BARC after program 3 digestion (1:300 dilution); (c) PR samples, where A is original PR (1:10000 dilution), B is PR after program 1 digestion (1:200 dilution), and C is PR after program 2 digestion (1:200 dilution); and (d) PR sample, where A is original PR (1:10000 dilution) and B is PR after program 3 digestion (1:100 dilution).

Figure 3b depicts the UV/visible absorbance of the BARC sample digested with the lower power program 3. It was found that strong absorption below 220 nm was still distinctive. This

Table 2. Microwave Programs Used for Closed-Vessel Digestion[a]

program 1				program 2				program 3			
step	power, %	time, min	pressure limit, psi	step	power, %	time, min	pressure limit, psi	step	power, %	time, min	pressure limit, psi
1	40	30	150	1	40	30	150	1	35	30	100
				2	55	30	150	2	35	30	100

[a] The sample volume is 0.25 mL. The first step in the digestion program uses 1.5 mL of HNO_3, and the second step uses 0.5 mL of H_2O_2.

Table 3. Digestion Efficiency (%) for Various Recipes Evaluated with the Total Dry Residual Method

program	BARC	PR
1	89.0	91.2
2	100	99.5
3	94.3	92.0

Table 4. Detection Limits of Lithographic Materials Digested with the Closed-Vessel Microwave Method and Analysis with ICPMS and ICP-OES[a]

	ICPMS		ICP-OES	
element	mass	ppb	wavelength, nm	ppb
Na	23	3.99	589.6	12.8
Al	27	0.55	396.2	2.3
Ca	44	19.6	396.8	2.3
Cr	52	1.13	267.7	1.6
Fe	57	6.21	259.9	3.3
Ni	60	0.21	231.6	4.1
Cu	65	0.10	324.8	2.6
Zn	66	0.79	213.9	2.8
Au	197	0.71	242.8	1.5
Pb	208	0.10	220.4	6.6
Sn	118	0.65	235.5	14.3
Pt	195	0.04	214.4	5.9
Cs	133	0.08		

[a] The detection limits are based on 3 times the standard deviation of the procedure blank ($n = 6$).

Table 5. Spike Recoveries (%) of BARC and PR Samples Treated by Closed-Vessel Microwave Digestion and Determined by ICPMS

	BARC	PR		BARC	PR
Na	132	98	Zn	116	106
Al	121	100	Au	111	103
Ca	142	187	Pb	108	109
Cr	91	87	Sn	97	89
Fe	127	117	Pt	104	88
Ni	110	125	Cs	101	112
Cu	107	100			

shows that the higher power used in program 2 was responsible for BARC decomposition. Other evidence can be found from the results of gravimetric method listed in Table 3. The results reveal that the BARC digestion efficiency with program 2 was absolutely complete (100%) as compared with other programs. Digestion by programs 1 and 3 could only achieve 89 and 94.3% efficiency, respectively. The somewhat positive correlation between the digestion efficiency from the total dry residual method and the exhibiting absorbance of the sample may provide a feasible means to identify the digestion possibility.

Table 6. Analytical Results of BARC and PR Samples Digested by the Closed-Vessel Microwave Method and Analysis with ICPMS

	BARC		PR	
element	ppb	RSD, %	ppb	RSD, %
Na	166 ± 7	4.2	298 ± 3	1.0
Na[a]	169 ± 3	1.8	280 ± 18	6.4
Al	151 ± 4	2.6	3.12 ± 0.18	5.8
Al[a]	161 ± 6	3.7	nd[b]	
Ca	169 ± 40	23.7	76.1 ± 3.9	5.1
Cr	1.95 ± 0.31	15.9	7.9 ± 0.6	7.6
Fe	7.62 ± 0.90	11.8	7.36 ± 1.21	16.4
Ni	1.01 ± 0.24	23.8	1.08 ± 0.06	5.6
Cu	1.56 ± 0.21	13.5	2.55 ± 0.16	6.3
Zn	4.16 ± 0.26	6.3	2.09 ± 0.31	14.8
Au	5.53 ± 0.67	12.1	12.1 ± 0.9	7.4
Pb	nd		nd	
Sn	0.51 ± 0.02	3.9	5.79 ± 0.53	9.2
Pt	nd		nd	
Cs	nd		nd	

[a] Analysis with ICP-OES. [b] nd, = not detected.

Parts c and d of Figure 3 show the UV/visible absorption spectra from 200 to 500 nm for the PR sample. It was found that the absorbance at 200−220 and 300−450 nm was still higher for both programs 1 and 3 and that the absorbance after program 2 digestion had lower intensity over the same spectrum. This result indicates that program 2 should also be suitable for PR digestion. Similar to the case of BARC digestion, the digestion efficiency was higher with program 2 (99.5%) as compared to the efficiency with programs 1 and 3 (91.2 and 92%, respectively). From these results, we have demonstrated that the UV/visible and gravimetric methods can serve as meaningful indicators to evaluate the digestion efficiency of the PR sample.

Analysis of Lithographic Materials. The analytical performance of the closed-vessel microwave digestion and instrumental determination method were evaluated in terms of detection sensitivity, spike recovery, and analytical reliability. The detection limits of these methods are defined as the analyte concentration that gives a signal intensity which is 3 times the standard deviation of the procedure blank ($n = 7$). It was estimated that the detection limits were in the ppb and sub-ppb levels for ICPMS and ppb levels for ICP-OES. As shown in Table 4, the detection limits of the ICPMS method was indeed better than those of the ICP-OES method, except for Ca and Fe. Polyatomic interference at m/z 44 (from $^{12}C^{16}O_2^+$) and 57 (from $^{40}Ar^{16}O^1H^+$) deteriorated the detection limits of Ca and Fe. This table generally implies that only ICPMS is suitable for sub-ppb determination.

Recovery tests were performed by spiking equivalent amounts of 5 ppb metals into the closed vessel, followed by the digestion

sequence and ICPMS determination. The results of the spike recovery tests for these metals are shown in Table 5. As can be seen, the spike recoveries of the closed-vessel method for all analytes except Ca ranged between 91 and 132% for BARC and 87 and 125% for PR. The recovery of Ca was not acceptable due to the polyatomic interference from CO_2^+ in ICPMS detection. The results of spike recoveries indicate the feasibility of applying the closed-vessel microwave digestion procedure and ICPMS multielement determination method for lithographic materials, except for Ca.

The proposed method has already been applied to the determination of metals in semiconductor lithographic samples. Table 6 shows the analytical results. The relative standard deviations (RSDs) for BARC and PR were within 23.8 and 16.4%, respectively, revealing that the analytical results are all within reasonably good precision. Although no commercial certified reference samples are available for both BARC and PR, the literature results,[23] obtained from open-focused microwave digestion and ICPMS analysis, are all in good agreement with this study. In addition, the analytical reliability of Na and Al is also verified by ICP-OES detection.

(23) Ko, F.-H.; Hsiao, L.-T.; Chou, C.-T.; Wang, M.-Y.; Wang, T.-K.; Sun, Y.-C.; Cheng, B.-J.; Yeng, S.; Dai, B.-T. *Proc. SPIE* **1999**, *V3677*, 907–917.

ACKNOWLEDGMENT

The authors thank the National Science Council, Taiwan, for financially supporting this research through Contract NSC89-2721-2317-200. They also thank Mr. Walter Den for comments on this paper.

Received for review June 21, 1999. Accepted September 21, 1999.

AC9906779